INDIAN JOURNAL OF SCIENCE AND TECHNOLOGY

RESEARCH ARTICLE

Numerical Investigation of Three-Dimensional Magnetohydrodynamic Flow of Ag – H_2O Nanofluid Over an Oscillating Surface in a Rotating Porous Medium

Rekha Devi[1]*, **Shilpa Sood**[2]

1 Research Scholar, Department of Mathematics and Statistics, Career Point University, Hamirpur, Himachal Pradesh, India
2 Associate Professor, Career Point University, Hamirpur, Himachal Pradesh, India

OPEN ACCESS

Received: 15-11-2023
Accepted: 23-01-2024
Published: 14-02-2024

Citation: Devi R, Sood S (2024) Numerical Investigation of Three-Dimensional Magnetohydrodynamic Flow of Ag – H_2O Nanofluid Over an Oscillating Surface in a Rotating Porous Medium. Indian Journal of Science and Technology 17(8): 679-690. https://doi.org/10.17485/IJST/v17i8.2892

* **Corresponding author**.

rekha111179@gmail.com

Funding: None

Competing Interests: None

Published By Indian Society for Education and Environment (iSee)

ISSN
Print: 0974-6846
Electronic: 0974-5645

Abstract

Objective: To investigate the three-dimensional flow of a nanofluid (Ag-water) over a stretchable vertical oscillatory sheet. This study involves considering fluctuating temperatures on the sheet and comparing them to the free stream temperature. The formulation of the unsteady boundary layer equations leading to the flow of nanofluid also takes into consideration the occurrence of the heterogeneous-homogeneous chemical reaction and thermal radiation. **Method:** The governing equations and the boundary conditions have been derived in a dimensionless form by using the appropriate transformations, and they are then solved using an EFDS (Explicit Finite Difference Scheme) in Matlab software. The Von-Neumann stability analysis is used to determine the method's stability requirements for constant sizes of the grid. **Findings:** The physical factors impact on the concentration fields, temperature distribution, and velocity distribution were obtained and are studied by graphs and described in extensive detail. Convergence and stability requirements are attained in order to achieve accurate solutions. **Novelty:** In this study fluctuations in the temperature and stretching velocity of sheet on three-dimensional magnetohydrodynamic flow of Ag – H_2O nanofluid over an oscillating surface through rotating porous are taken into account. Impacts of porous media permeability, velocity slip, magnetic fields, nanoparticle volume fraction, heat radiation, rotation, and homogeneous and heterogeneous chemical reaction parameters had all been attempted to be determined.

Keywords: Oscillatory Surface; Heat transmission; Nonlinear PDE; Explicit Finite Difference Scheme; Nanoparticle

1 Introduction

The investigation of convective heat and mass transfer processes in the MHD boundary layer region, where flow is induced by the surface's stretching as well as its periodic

oscillation and rotation, is crucial for both industry and technology. Numerous sectors, including those that produce food, paper, cosmetics, polymers, and oil exploration, depend extensively on the research of nanofluid flow past oscillatory flows. They serve a variety of purposes in biology, including regulating blood flow during surgery, modeling lung function, and dispensing chemicals and blood in biochemical and clinical labs. The energy dissipation function and porous medium are taken into account in the momentum and energy equations by Lund et al.[1], who studied the effects of high temperature on the porous surface. The combined impacts of chemical reaction and thermal radiation on MHD free convective heat as well as the mass transfer effects of the nanofluid have been examined by Arulmozhi et al.[2] on an infinite moving vertical plate. Anuar[3] studied the flow and heat transfer of carbon nanotubes over an exponentially stretching/shrinking sheet with homogeneous–heterogeneous reactions. Alsani et al.[4] deliberated on the joint effects of the inclined functional magnetic field, the absorbent stretching surface, the mass transportation, and the radiative warming on a micropolar flow. Jalili, et al.[5] studied the effect of thermo-diffusion, electrical field, and nonlinear thermal radiation. Thermal radiant heat transfer has several industrial applications, and the analysis of radiation heat transfer in non-Newtonian fluids under different conditions has been widely studied. In the literature, we also come across various publications that discussed the impact of radiation and magnetic fields on fluid flow past stretched surfaces. Hussain et al.[6,7] looked at the heat transfer characteristics of a three-dimensional water-based magneto-hydrodynamic rotating nanofluid flow across a linear stretching sheet. Nasirzadehroshenin et al.[8] demonstrated that carbon nanotubes could transport heat. Shoaib et al.[9] investigated the heat and mass transport in a rotating flow of MHD hybrid nanofluid with thermal radiation over a stretching sheet by utilizing the power of the Lobatto IIIA method, which is based on numerical computing.

Farooq et al. conducted a study on the MHD flow induced by oscillating surfaces that took into consideration the Soret and Dufour effects[10]. Khan et al. looked into electrical MHD Carreau nanofluid over porous oscillatory stretching surface with variable thermal conductivity and applications of thermal extrusion system[11]. Kumar et al.[12] effects of Joule and viscous dissipation in three-dimensional flow of nanoliquid have been addressed in slip flow regime under time dependent rotational oscillations. To the best of our knowledge, an oscillating stretching sheet with an MHD rotating boundary layer flow of Ag-water nanofluid has not yet been explored. This study fills the gap in the literature by providing details on the mass and heat transfer processes over such surfaces, which are immensely important to business, technology, and research.

Mathematical Formulation of the problem

We assume the flow of an unsteady, incompressible, viscous, electrically conducted Ag-water nano-fluid in an MHD rotating boundary layer by an oscillating stretchable sheet. It is believed that the sheet is being stretched with velocity $u = a\,x\,cos\,(\omega t)$ in the x direction. Additionally, it is supposed that the sheet maintains a constant temperature and that the complete system is at rest for $t \leq 0$. For $t > 0$, it is believed that the sheet is oscillating harmonically with frequency (Ω') of the rotating fluid; both the fluid and the sheet are in a body rotation state. Homogeneous chemical reactions have the following equation: r+2s→3s, rate=$k_c C_r C^2$. Heterogeneous chemical reactions on catalyst surfaces have the equation: r→s, rate=$k_s C_r$, where C_r, $C_s$denotes the chemical species.

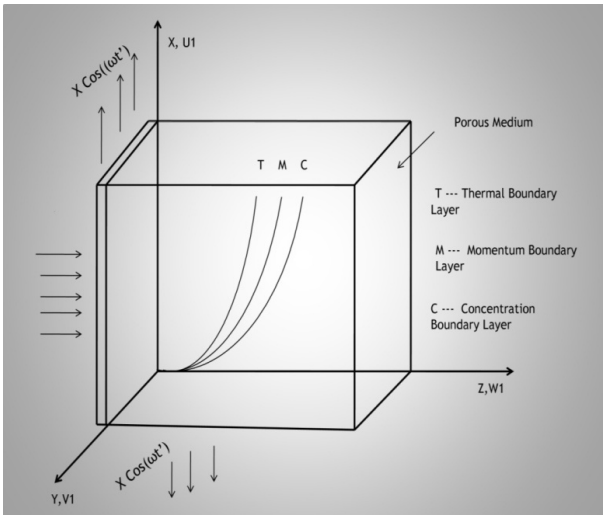

Fig 1. Physical configuration of the study

We formulate the governing equations for the unsteady boundary layer within a rotating frame of reference, as elucidated by Hussain[13] are

$$\frac{\partial u^1}{\partial x}+\frac{\partial v^1}{\partial y}+\frac{\partial w^1}{\partial z}=0 \tag{1}$$

$$\frac{\partial u^1}{\partial t}+u^1\frac{\partial u^1}{\partial x}+v^1\frac{\partial u^1}{\partial y}+w^1\frac{\partial u^1}{\partial z}=\nu_{n_0}\frac{\partial^2 u^1}{\partial z^2}-\frac{\sigma_{n_0}B*^2}{\rho_{n_0}}u^1-\frac{\mu_{n_0}u^*}{\rho_{n_0}}+2\Omega^{'}v^1+\frac{g(\rho\beta_T)_{n_0}}{\rho_{n_0}k}(T-T_\infty) \tag{2}$$

$$\frac{\partial v^1}{\partial t}+u^1\frac{\partial v^1}{\partial x}+v^1\frac{\partial v^1}{\partial y}+w^1\frac{\partial v^1}{\partial z}=\nu_{n_0}\frac{\partial^2 v^1}{\partial z^2}-\frac{\sigma_{n_0}B*^2}{\rho_{n_0}k}v^1-2\nu\Omega^{'}u^1 \tag{3}$$

$$\frac{\partial T}{\partial t}+u^1\frac{\partial T}{\partial x}+v^1\frac{\partial T}{\partial y}+w^1\frac{\partial T}{\partial z}=\alpha_{n_0}\frac{\partial^2 T}{\partial z^2}+\frac{1}{(\rho c_p)_{n_0}}\frac{\partial q_r}{\partial z}-\frac{\sigma_{n_0}B*^2}{\rho_{n_0}}\left(\left(\frac{\partial u^1}{\partial z}\right)^2+\left(\frac{\partial v^1}{\partial z}\right)^2\right) \tag{4}$$

$$\frac{\partial C_r}{\partial t}+u^1\frac{\partial C_r}{\partial x}+v^1\frac{\partial C_r}{\partial y}+w^1\frac{\partial C_r}{\partial z}=D_r\frac{\partial^2 T}{\partial z^2}-k_cC_r{C_s}^2, \tag{5}$$

$$\frac{\partial C_s}{\partial t}+u^1\frac{\partial C_s}{\partial x}+v^1\frac{\partial C_s}{\partial y}+w^1\frac{\partial C_s}{\partial z}=D_s\frac{\partial^2 T}{\partial z^2}-k_cC_s{C_r}^2, \tag{6}$$

The prescribed form for the initial and boundary conditions relevant to the considered problem is as follows:

$t^{'}\le 0,\ u^1=v^1=w^1=C_s=0;\ T=T_\infty,\ C_r=a_0,\ everywhere,$

$t>0,\ x=0;\ u^1=v^1=w^1=C_s=0,\ T=T_\infty,\ C_r=a_0,$

$y=0;\ u^1=v^1=w^1=\ 0,\ C_s=0,\ T=T_\infty,\ C_r=a_0$

$z=0;\ u^1=cos(\omega t^{'})+L_1\frac{\partial u^1}{\partial z},\ v^1=w^1=0,$

$T=T_\infty+(T_w^*-T_\infty)\,cos\left(\omega t^{'}\right),\ D_r\frac{\partial(C_r)}{\partial z}=k_cC_r,\ D_s\frac{\partial(C_s)}{\partial z}=-k_sC_r,$

$$Z\longrightarrow\infty;\ u^1=v^1=0=C_s=0,T=T_\infty,C_r=a_0 \tag{7}$$

Here, u^1, v^1, and w^1 correspond to components of the velocity along the x, y, and z axes respectively. g, β_T, ρ, c_p, ν, α, C_r, C_s, σ^*, q_r and k^* represent the acceleration due to gravity, volume expansion coefficient, density, the specific heat capacity, the kinematic viscosity, thermal diffusivity, coefficient of thermal expansion, Stefan-Boltzmann constant, radiative heat flux, and mean absorption coefficient respectively.

Thermophysical properties of nanofluid stated as[14,15]

Dynamic Viscosity of fluid $\mu_{n_0}=\frac{\mu_{f_0}}{1-(\varphi)^{2.5}}$

Nanofluid Effective density $\rho^{'}_{n_0}=(1-\phi)\rho^{'}_{f_0}+(\phi)\rho^{'}_{s0}$

Nanofluid Effective heat capacity $(\rho^{'}_Cp)_{n0}=1-(\phi)(\rho^{'}_Cp)_{f0}+(\varphi)(\rho^{'}_Cp)_{s0}$

Effective thermal conductivity of nanofluid

$$\frac{\kappa^{'}_{n0}}{\kappa^{'}_{f0}}=\frac{\kappa^{'}_{s0}+(n-1)\kappa^{'}_{f0}+(n-1)\varphi(\kappa^{'}_{f0}-\kappa^{'}_{s0})}{\kappa^{'}_{s0}+(n-1)(\kappa^{'}_f-\kappa^{'}_{s0})}$$

Electrical conductivity of nanofluid:

$$\frac{\sigma^{'}_{n0}}{\sigma^{'}_{f0}}=1+\frac{3\left(\frac{\sigma^{'}_s}{\sigma^{'}_f}-1\right)\phi}{\frac{\sigma^{'}_{s0}}{\sigma^{'}_{f0}}-2-\left(\frac{\sigma^{'}_{s0}}{\sigma^{'}_{f0}}-1\right)\phi}$$

Thermal expansion coefficient of Nanofluid $\rho\beta_{Tn0} = (1-\phi)\rho^{'}\beta_{Tf0} + \phi\rho^{'}\beta_{Ts0}$

Equations (1), (2), (3), (4), (5) and (6) and boundary conditions Equation (7) after using the aforementioned non-dimensional quantities become

$$U_1 = z\sqrt{\frac{1}{\nu_{f0}c}}, \Phi_f = \frac{C_r}{a_0}, V_1 = z\sqrt{\frac{1}{\nu_{f0}c^{'}}}, Y = y\sqrt{\frac{c^{'}}{\nu_{f0}}}, W_1 = w^*\sqrt{\frac{1}{\nu_{f0}c^{'}}}, X = x\sqrt{\frac{c^{'}}{\nu_{f0}}},$$

$$Z = z\sqrt{\frac{c^{'}}{\nu_{f0}}}, t^{'} = tc^{'}, \omega = \frac{\omega^{'}}{c^{'}}, \theta = \frac{T-T_\infty}{T_w^* - T_\infty}, \Phi_s = \frac{C_s}{a_0},$$

The following governing equations are obtained:

$$\frac{\partial U_1}{\partial X} + \frac{\partial V_1}{\partial Y} + \frac{\partial W_1}{\partial Z} = 0, \tag{8}$$

$$\frac{\partial U_1}{\partial t'} + U_1\frac{\partial U_1}{\partial X} + V_1\frac{\partial U_1}{\partial Y} + W_1\frac{\partial U_1}{\partial Z} = \frac{1}{S_1S_2}\frac{\partial^2 U_1}{\partial Z^2} - \frac{MS_3}{S_2}U_1 - \frac{KU_1}{S_1S_2} + RV_1 + \frac{GrS_4}{S_2}\theta \tag{9}$$

$$\frac{\partial V_1}{\partial t'} + U_1\frac{\partial V_1}{\partial X} + V_1\frac{\partial U_1}{\partial Y} + W_1\frac{\partial U_1}{\partial Z} = \frac{1}{S_1S_2}\frac{\partial^2 V_1}{\partial Z^2} - \frac{MS_3}{S_2}V_1 - \frac{KV_1}{S_1S_2} - RU_1, \tag{10}$$

$$\frac{\partial \theta}{\partial t'} + U_1\frac{\partial \theta}{\partial X} + V_1\frac{\partial \theta}{\partial Y} + W_1\frac{\partial \theta}{\partial Z} = \frac{1}{Pr}\left(\frac{S_6}{S_5} + \frac{Ra}{S_5}\right)\frac{\partial^2 T}{\partial Z^2} + \frac{MA_3Ec}{S_5}\left(U_1^2 + V_1^2\right)) - \frac{MS_3Ec}{S_5}\left(\left(\frac{\partial U_1}{\partial Z}\right)^2 + \left(\frac{\partial V_1}{\partial Z}\right)^2\right) \tag{11}$$

$$\frac{\partial \Phi_f}{\partial t'} + U_1\frac{\partial \Phi_f}{\partial x} + V_1\frac{\partial \Phi_f}{\partial y} + W_1\frac{\partial \Phi_f}{\partial z} = \frac{1}{Sc}\frac{\partial^2 \Phi_f}{\partial Z^2} - K_c\Phi_f\Phi_s^2, \tag{12}$$

$$\frac{\partial \Phi_s}{\partial t'} + U_1\frac{\partial \Phi_s}{\partial X} + V_1\frac{\partial \Phi_s}{\partial Y} + W_1\frac{\partial \Phi_s}{\partial Z} = \frac{\delta}{Sc}\frac{\partial^2 \Phi_s}{\partial Z^2} + K_c\Phi_f\Phi_s^2, \tag{13}$$

Where $S_1 = 1-(\phi)^{2.5}, S_2 = (1-\phi) + \phi\frac{\rho_{s0}^{'}}{\rho_{f0}}$, $S_3 = 1 + \frac{3\left(\frac{\sigma_{s0}^{'}}{\sigma_{f0}^{'}} - 1\right))\phi}{\left(\frac{\sigma_{s0}^{'}}{\sigma_{f0}^{'}} + 2\right) - \left(\frac{\sigma_{s0}^{'}}{\sigma_{f0}^{'}} - 1\right)\phi}$

$S_4 = (1-\phi) + \phi\frac{\rho(\beta_T)_{s0}}{\rho(\beta_T)_{f0}}, S_5 = (1-\phi) + \phi\frac{(\rho C_p)_{s0}}{(\rho C_p)_{f0}}$, $S_6 = \frac{k_{n0}}{k_{f0}}$

Upon implementing the aforementioned non-dimensional transformations, the boundary conditions take the following form:

$$t^{'} \le 0\left(U_1 = V_1 = W_1 = \theta = \Phi_s = 0, \Phi_f = 1,\right) \quad everywhere,$$

$$t > 0, \left(X = 0; U_1 = V_1 = W_1 = \theta = \Phi_s = 0, \Phi_f = 1,)\right),$$

$$for\, Y = 0; U_1 = cos\left(\omega t^{'}\right)X + V_s\frac{\partial V}{\partial Z}, V_1 = W_1$$

$$Z=0;\ U_1=V_1=W_1=\theta=\Phi_s=0,\Phi_f=1\ \theta=cos(\omega t^{'});\ \frac{\partial(\Phi_f)}{\partial Z}=K_s\Phi_f,\ \frac{\partial(\Phi_s)}{\partial Z}=-K_s\Phi_f$$

$$Z\longrightarrow\infty;\ U^1=V^1=0=\theta=\Phi_s=0,\ \Phi_f=1$$

In the aforementioned equations, the dimensionless parameters introduced are given as follows:

$$M=\frac{(B^*)^2\sigma}{c},K=\frac{\nu_{f0}}{kc},R=\frac{2\Omega^{'}}{c},Gr_x=\frac{(g\beta^*)_{f0}(T_w-T_\infty)}{\rho_{f0}\sqrt{\nu_f c^3}},Ra=\frac{16\sigma_* T_\alpha^3}{3k^* k_{f0}}Sc=\frac{\nu_{f0}}{D_B},$$

$$\delta=\frac{D_s}{D_r},K_c=\frac{k_c a_0^2}{c},Pr=\frac{\nu_{f0}}{\alpha_{f0}},V_s=L_1\sqrt{\frac{c}{\nu}},Ec=\frac{\nu_{f0}c}{(c_p)_{f0}(T_w-T_\infty)},K_s=\frac{k_s}{D_r}\sqrt{\frac{\nu_{f0}}{c}}$$

Skin friction coefficients(C_{fx}^*, C_{fy}^*), local Nusselt number Nu_x and Sherwood numbers (Sh_{C_r}, Sh_{C_s}) are given as follows:

$$C_{fx}^*=\frac{\tau_{\omega y}}{\rho_{f0}u_\omega^2},C_{fy}^*=\frac{\tau_{\omega y}}{\rho_{f0}u_\omega^2},\ Nux=\frac{xq_\omega}{k_{f0}\,(T_w-T_\infty)},Sh_{C_r}=\frac{xj_{\omega g}}{D_r a_0},Sh_{C_s}=\frac{xj_{\omega r}}{D_s a_0},$$

$$\tau_{\omega x}=\mu_{nf}\left(\frac{\partial u}{\partial z}\right)_{Z=0},\tau_{\omega y}=\mu_{n0}\left(\frac{\partial v}{\partial z}\right)_{Z=0},q_{\omega y}=\kappa_{n0}^{'}\left(\frac{\partial T}{\partial z}\right)_{Z=0}+(q_r)_{Z=0}$$

$$j_{\omega r}=-D_r\left(\frac{\partial C_r}{\partial z}\right)_{Z=0},\ \ j_{\omega s}=-D_s\left(\frac{\partial C_s}{\partial z}\right)_{Z=0}$$

Upon implementation of non-dimensional transformations, we have the following expression:

$$C_{fx}^*=\frac{1}{S_1\left(Xcos\omega t^{'})^2\right)}\left(\frac{\partial U}{\partial Z}\right)_{Z=0},C_{fY}^*=\frac{1}{S_1\left(Xcos\omega t^{'})^2\right)}\left(\frac{\partial V}{\partial Z}\right)_{Z=0},$$

$$Nu_X=X(-S6-Ra)\left(\frac{\partial\theta}{\partial Z}\right)_{Z=0},Sh_{\Phi_f}^*=X\left(\frac{\partial\Phi_f}{\partial Z}\right)_{Z=0},Sh_{\Phi_s}^*=X\left(\frac{\partial\Phi_s}{\partial Z}\right)_{Z=0}$$

2 Methodology

An explicit finite difference technique (EFDS) was used to solve nonlinear coupled partial differential equations with the aid of the initial and boundary conditions. The finite difference equations system shown below is created utilizing EFDS.

$$\frac{U_{1_{(e,m,g)}}^{n+1}-U_{1_{(e-1,m,g)}}^{n+1}}{\Delta X}+\frac{V_{1_{(e,m,g)}}^{n+1}-V_{1_{(e,m-1,g)}}^{n+1}}{\Delta Y}+\frac{W_{1_{(e,m,g)}}^{n+1}-W_{1_{(e,m,g-1)}}^{n+1}}{\Delta Z}=0 \tag{14}$$

$$\begin{aligned}&\frac{U_{1_{(e,m,g)}}^{n+1}-U_{1_{(e,m,g)}}^{n}}{\Delta t'}+U_{1_{(e,m,g)}}^{n}\frac{U_{1_{(e,m,g)}}^{n}-U_{1_{(e-1,m,g)}}^{n}}{\Delta X}+V_{1_{(e,m,g)}}^{n}\frac{U_{1_{(e,m,g)}}^{n}-U_{1_{(e,m-1,g)}}^{n}}{\Delta Y}\\&+W_{1_{e,m,g}}^{n}\frac{U_{1_{e,m,g+1}}^{n}-U_{1_{e,m,g}}^{n}}{\Delta Z}=\frac{1}{S_1S_2}\frac{U_{1_{(e,m,g-1)}}^{n}-2U_{1_{(e,m,g)}}^{n}+U_{1_{(e,m,g+1)}}^{n}}{\Delta Z^2}\\&-\frac{MS_3}{S_2}U_{1_{(e,m,g)}}^{n}-\frac{K}{S_1S_2}U_{1_{(e,m,g)}}^{n}+RV_{1_{(e,m,g)}}^{n}+\frac{GrS_4\theta_{(e,m,g)}^{n+1}}{S_2}\end{aligned} \tag{15}$$

$$\frac{V_{1(e,m,g)}^{n+1}-V_{1(e,m,g)}^{n}}{\Delta t'}+V_{1(e-1,m,g)}^{n}\frac{V_{1(e,m,g)}^{n+1}-V_{1(e-1,m,g)}^{n}}{\Delta X}+V_{1(e,m,g)}^{n}\frac{V_{1(e,m,g)}^{n+1}-V_{1(e,m-1,g)}^{n}}{\Delta Y}$$
$$+W_{1(e,m,g)}^{n}\frac{V_{1(e,m,g+1)}^{n+1}-U_{1(e,m,g)}^{n}}{\Delta Z}=\frac{1}{S_1S_2}\frac{V_{1(e,m,g-1)}^{n}-2V_{1(e,m,g)}^{n}+V_{1(e,m,g+1)}^{n}}{\Delta Z^2} \quad (16)$$
$$-\frac{MS_3}{S_2}V_{1(e,m,g)}^{n}-\frac{K}{S_1S_2}V_{1(e,m,g)}^{n}++RU_{1(e,m,g)}^{n}$$

$$\frac{\theta_{e,m,g}^{n+1}-\theta_{e,m,g}^{n}}{\Delta t'}+U_{1e,m,g}^{n}\frac{\theta_{e,m,g}^{n+1}-\theta_{e-1,m,g}^{n}}{\Delta X}+V_{1e,m,g}^{n}\frac{\theta_{e,m,g}^{n+1}-\theta_{e,m-1,g}^{n}}{\Delta Y}+(W^1)_{e,m,g}^{n}\frac{\theta_{e,m,g+1}^{n+1}-\theta_{e,m,g}^{n}}{\Delta Z}$$
$$=\frac{1}{Pr}\left(\frac{S_6}{S_5}+\frac{Ra}{S_5}\right)\frac{\theta_{(e,m,g-1)}^{n}-2\theta_{e,m,g}^{n}+\theta_{e,m,g+1}^{n}}{\Delta Z^2}+\frac{MEcS_3}{S_5}\left(U_{1(e,m,g)}^{n})^2+V_{1(e,m,g)}^{n})^2\right) \quad (17)$$
$$+\frac{Ec}{S_1S_5}\left(\left(\frac{U_{1(e,m,g+1)}^{n}-U_{1(e,m,g)}^{n}}{\Delta Z}\right)^2+\left(\frac{V_{1(e,m,g+1)}^{n}-V_{1(e,m,g)}^{n}}{\Delta Z}\right)^2\right)$$

$$\frac{\Phi_{f(e,m,g)}^{n+1}-\Phi_{f(e,m,g)}^{n}}{\Delta t'}+U_{1f(e,m,g)}^{n}\frac{\Phi_{f(e,m,g)}^{n+1}-\Phi_{f(e-1,m,g)}^{n}}{\Delta X}+V_{1(e,m,g)}^{n}\frac{\Phi_{f(e,m,g)}^{n+1}-\Phi_{f(e,m-1,g)}^{n}}{\Delta Y}+W_{1(e,m,g)}^{n}\frac{\Phi_{f(e,m,g+1)}^{n+1}-\Phi_{f(e,m,g)}^{n}}{\Delta Z} \quad (18)$$
$$=\frac{1}{Sc}\frac{\Phi_{s(e,m,g-1)}^{n}-2\Phi_{s(e,m,g)}^{n}-\Phi_{s(e,m,g+1)}^{n}}{\Delta Z^2}-K_c\Phi_{s(e,m,g)}^{n}(\Phi_{s(e,m,g)}^{n})^2$$

$$\frac{\Phi_{se,m,g}^{n+1}-\Phi_{s(e,m,g)}^{n}}{\Delta t'}+U_{1s(e,m,g)}^{n}\frac{\Phi_{s(e,m,g)}^{n+1}-\Phi_{e-1,m,g}^{n}}{\Delta X}+V_{1(e,m,g)}^{n}\frac{\Phi_{s(e,m,g)}^{n+1}-\Phi_{s(e,m-1,g)}^{n}}{\Delta Y}+W_{1(e,m,g)}^{n}\frac{\Phi_{s(e,m,g+1)}^{n+1}-\Phi_{e,m,g}^{n}}{\Delta Z} \quad (19)$$
$$=\frac{1}{Sc}\frac{\Phi_{s(e,m,g-1)}^{n}-2\Phi_{s(e,m,g)}^{n}-\Phi_{s(e,m,g+1)}^{n}}{\Delta Z^2}+K_c\Phi_{f(e,m,g)}^{n}(\Phi_{s(e,m,g)}^{n})^2$$

Initial and boundary conditions using finite difference approximation gives:

$$U_{1(e,m,g,0)}=V_{1(e,m,g,0)}=W_{1(e,m,g,0)}=\theta_{(e,m,g,0)}=\Phi_s(e,m,g,0)=0,\Phi_f(e,m,g,0)$$
$$=1,U_{1(0,m,g,t')}=V_{1(0,m,g,t')}=W_{1(0,m,g,t')}=\theta_{(0,m,g,t')}=\Phi_s(0,m,g,t')=0,\Phi_f(0,m,g,t')=1$$

$$U_{1(0,m,g,t')}=V_{1(0,m,g,t')}=W_{1(0,m,g,t')}=\theta_{(0,m,g,t')}=\Phi_s(0,m,g,t')=0,\Phi_f(0,m,g,t')=1$$

$$U_{1(e,0,k,t')}=V_{1(e,0,g,t')}=W_{1(e,0,g,t')}=\theta(e,0,g,t')=\Phi_s(e,0,g,t')=0,\Phi_f(e,0,g,t')=1$$

$$U_{1(e,0,g,t')}=Vs\frac{U_{1(e,0,g,t')}-V_{1(e,0,g,t')}}{\Delta Z}+X(\iota)cos(\omega t'),\theta_{(e,m,0,t')}=cos(\omega t'),$$

$$\frac{\Phi_f\left(e,m,1,t'\right)-\Phi_f\left(e,0,g,t'\right)}{\Delta Z}=K_s\Phi_f\left(e,m,0,t'\right),$$

$$\delta\frac{\Phi_s(e,m,1,t')-\Phi_s(e,0,g,t')}{\Delta Z}=K_s\Phi_f(e,g,0,t') \quad (20)$$

The prescribed maximum values are as follows: X_{max} = 100, Y_{max} = 100 and Z_{max} = 25. The selection of the approximate Z_{max} value, corresponding to Z = ∞, ensures that it resides significantly beyond the boundaries of momentum, energy, and concentration boundary layers.

2.1 Stability and Convergence

We used an EFDS, it is important to satisfy the convergence and stability assumptions in order to attain valid results. The Von-Neumann stability analysis is used to determine the method's stability requirements for constant sizes of the grid.

$$U_1 = N(t^{'})e^{-\iota T^{'}X}e^{-\iota\rho^{'}Z}e^{-\iota\upsilon^{'}Z}, V_1 = \Psi(t^{'})e^{-\iota T^{'}X}e^{-\iota\rho^{'}Z}e^{-\iota\upsilon^{'}Z}\theta = \zeta(t^{'})e^{-\iota T^{'}X}e^{-\iota\rho^{'}Z}e^{-\iota\upsilon^{'}Z},$$

$$\phi_f = \varphi(t^{'})e^{-\iota T^{'}X}e^{-\iota\rho^{'}Z}e^{-\iota\upsilon^{'}Z}, \phi_s = \Upsilon(t^{'})e^{-\iota T^{'}X}e^{-\iota\rho^{'}Z}e^{-\iota\upsilon^{'}Z}$$

Upon substituting the aforementioned expressions, the system of equations is given as follows:

$$U_1 = N^*(t^{'})e^{-\iota T^{'}X}e^{-\iota\rho^{'}Z}e^{-\iota\upsilon^{'}Z}, V_1 = \Psi^*(t^{'})e^{-\iota T^{'}X}e^{-\iota\rho^{'}Z}e^{-\iota\upsilon^{'}Z}\theta = \zeta^*(t^{'})e^{-\iota T^{'}X}e^{-\iota\rho^{'}Z}e^{-\iota\upsilon^{'}Z},$$

$$\phi_f = \varphi^*(t^{'})e^{-\iota T^{'}X}e^{-\iota\rho^{'}Z}e^{-\iota\upsilon^{'}Z}, \phi_s = \Upsilon^*(t^{'})e^{-\iota T^{'}X}e^{-\iota\rho^{'}Z}e^{-\iota\upsilon^{*}Z}$$

$$N^* = A^*N + B^*\Psi + I^*\zeta, \psi^* = E^*N + F^*\Psi, \zeta^* = G^*\Theta + G_1^*N + G_2^*\Psi, \varphi^* = L^*\varphi, \chi^* = M^*\chi + N^*\varphi,, I^* = C^*G^*$$

The above system can be expressed in matrix form as $A^{*}X = B^{*}$. In the coefficient matrix A^{*}, the entries for are represented as follows:

$$\begin{aligned} A^* &= 1 - U_1(1 - e^{-\iota T^{'}\Delta X})\tfrac{\Delta t^{'}}{\Delta X} - V_1(1 - e^{-\iota\rho^{'}\Delta Y})\tfrac{\Delta t^{'}}{\Delta Y} - W_1(1 - e^{-\iota\upsilon^{'}\Delta Z})\tfrac{\Delta t^{'}}{\Delta Z} + \\ &\tfrac{2}{S_1S_2}\tfrac{\Delta t^{'}}{\Delta Z^2}(Cos\upsilon^{'}\Delta Z) - 1) - \tfrac{S_3}{S_2}M\Delta t^{'} - \tfrac{K}{S_1S_2}\Delta t^{'} + G_1^*, \\ B^* &= R\Delta t^{'} + G_2^*, C^* = Gr\tfrac{S_4}{S_2}, E^* = -R\Delta t^{'}, M^* = -K_ch^2, \end{aligned}$$

$$F^* = 1 - U_1(1 - e^{-\iota T^{'}\Delta X})\frac{\Delta t^{'}}{\Delta X} - V_1(1 - e^{-\iota\rho^{'}\Delta Y})\frac{\Delta t^{'}}{\Delta Y} - W_1(1 - e^{-\iota\upsilon^{'}\Delta Z})\frac{\Delta t^{'}}{\Delta Z} + \frac{2}{S_1S_2}\frac{\Delta t^{'}}{\Delta Z^2}(Cos\upsilon^{'}\Delta Z) - 1)\frac{A_3}{A_2}M\Delta t^{'} - \frac{K}{A_1A_2}\Delta t^{'}$$

$$G^* = 1 - U_1(1 - e^{-\iota T\Delta X})\frac{\Delta t^{'}}{\Delta X} - V_1(1 - e^{-\iota\rho^{'}\Delta Y})\frac{\Delta t^{'}}{\Delta Y} - W_1(1 - e^{-\iota\upsilon^{'}\Delta Z})\frac{\Delta t^{'}}{\Delta Z} + 2\frac{1}{Pr}\left(\frac{S_6}{S_5} + \frac{Ra}{S_5}\right)\frac{\Delta t^{'}}{\Delta Z^2}(Cos\upsilon^{'}\Delta Z) - 1)$$

$$G_1^* = \frac{Ec}{S_1S_5}\left(e^{\upsilon^{'}\Delta Z} - 1\right)^2\frac{\Delta t^{'2}}{\Delta Z} + \frac{EcMS_3}{S_1S_5}\Delta t^{'}U_1, G_2^{'} = \frac{Ec}{S_1S_5}\left(e^{\upsilon^{'}T\Delta Z} - 1\right)^2\frac{\Delta t^{'2}}{\Delta Z} + \frac{EcMS_3}{S_1A_5}\Delta t^{'}V_1$$

$$L^* = 1 - U_1(1 - e^{-\iota T^{'}\Delta X})\frac{\Delta t^{'}}{\Delta X} - V_1(1 - e^{-\iota\rho^{'}\Delta Y})\frac{\Delta t^{'}}{\Delta Y} - W_1(1 - e^{-\iota\upsilon^{'}\Delta Z})\frac{\Delta t^{'}}{\Delta Z} + \frac{2}{Sc}\frac{\Delta t^{'}}{\Delta Z^2}(Cos\upsilon^{'}\Delta Z) - 1) + K_ch^2$$

$$N^* = 1 - U_1(1 - e^{-\iota T^{'}\Delta X})\frac{\Delta t^{'}}{\Delta X} - V_1(1 - e^{-\iota\rho^{'}\Delta Y})\frac{\Delta t^{'}}{\Delta Y} - W_1(1 - e^{-\iota\upsilon^{'}\Delta Z})\frac{\Delta t^{'}}{\Delta Z} + \frac{2}{Sc}\frac{\Delta t^{'}}{\Delta Z^2}(Cos\upsilon^{'}\Delta Z) - 1)$$

The Von-Neumann stability analysis is used to determine the method's stability requirements for constant sizes of the grid, write in unique way.

$$\lambda_1^* = 1 - a^1(1 - e^{-\iota T^{'}\Delta X}) - b^1(1 - e^{-\iota\rho^{'}\Delta Y}) - c^1(1 - e^{-\iota\upsilon^{'}\Delta Z}) + \frac{2}{S_1S_2}D(Cos\upsilon^{'}\Delta Z) - 1) - \frac{S_3}{S_2}M\Delta t^{'} - \frac{K}{S_1S_2}\Delta t^{'} + G_1^*$$

$$\lambda_2^* = 1 - a^1(1 - e^{-\iota T^{'} \Delta X}) - b^1(1 - e^{-\iota \rho^{'} \Delta Y}) - c^1(1 - e^{-\iota \upsilon^{'} \Delta Z}) + \frac{2}{S_1 S_2} D(Cos\upsilon^{'} \Delta Z) - 1) \frac{S_3}{S_2} M \Delta t^{'} - \frac{K}{S_1 S_2} \Delta t^{'} - \iota R \Delta t^{'},$$
$$\lambda_3^* = G^*, \lambda_4^* = L^*, \lambda_5^* = N*$$

In λ_{1^*} and λ_{2^*}, $a^1 = \frac{\triangle t'}{\triangle X}$, $b^1 = \frac{\triangle t'}{\triangle Y}$, $c^1 = \frac{\triangle t'}{\triangle Z}$ *and* $d^1 = \frac{\triangle t'}{\triangle Z^2}$,

for the scheme to maintain stability.

It is imperative that every eigen value must be less than unity

$$|U_1|\left(\frac{\Delta t^{'}}{\Delta X}\right) + |V_1|\left(\frac{\Delta t^{'}}{\Delta Y}\right) + |W_1|\left(\frac{\Delta t^{'}}{\Delta Z}\right) + \frac{2\Delta t^{'}}{S_1 S_2 \Delta Z^2} + \frac{S_3 M \Delta t^{'}}{2S_2} + \frac{K}{2S_1 S_2} - \iota R \Delta t^{'} \leq 1$$

$$|U_1|\left(\frac{\Delta t^{'}}{\Delta X}\right) + |V_1|\left(\frac{\Delta t^{'}}{\Delta Y}\right) + |W_1|\left(\frac{\Delta t^{'}}{\Delta Z}\right) + \frac{2\Delta t^{'}}{S_1 S_2 \Delta Z^2} + \frac{S_3 M \Delta t^{'}}{2S_2} + \frac{K}{2S_1 S_2} + \iota R \Delta t^{'} \leq 1$$

$$|U_1|\left(\frac{\Delta t^{'}}{\Delta X}\right) + |V_1|\left(\frac{\Delta t^{'}}{\Delta Y}\right) + |W_1|\left(\frac{\Delta t^{'}}{\Delta Z}\right) + \frac{2}{Pr}\left(\frac{S_6}{S_5} + \frac{Ra}{5}\right)\frac{\Delta t^{'}}{\Delta Z^2} \leq 1$$

$$|U_1|\left(\frac{\Delta t^{'}}{\Delta X}\right) + |V_1|\left(\frac{\Delta t^{'}}{\Delta Y}\right) + |W_1|\left(\frac{\Delta t^{'}}{\Delta Z}\right) + \frac{2\Delta t^{'}}{Sc\Delta Z^2} + \Delta t^{'} K_c\left(\phi_s^2\right) \leq 1$$

$$|U_1|\left(\frac{\Delta t^{'}}{\Delta X}\right) + |V_1|\frac{\Delta t^{'}}{\Delta Y} + |W_1|\left(\frac{\Delta t^{'}}{\Delta Z}\right) + \frac{2\delta \Delta t^{'}}{Sc\Delta Z^2} \leq 1$$

3 Results and Discussion

The profiles of primary velocity (U_1), secondary velocity (V_1), homogeneous species concentration (Φ_f), heterogeneous species concentration (Φ_s) and fluid temperature (θ) were plotted, by assigning values to relevant parameters. In order to demonstrate the significance of the oscillation parameter ω, a comparison study is provided for two situations, NFNF (ω = 0.0) and FNF (ω = 0.5). The findings are in excellent agreement when compared to the findings of Kumar et al.[12], Kumar & Sood[16]

Table 1. Comparisonofskin frictioncoefficients (C^*_{fX}, C^*_{fY}) and local Nusselt number Nu_x of Ra at ω = 0, Vs = 1, Kc = 0.5, ϕ = 0.1, R = 0.5, M = 1, K = 1.5, K_s = 3, R = 0.5, M = 1, Ec = 0.001, K = 1.5, and Gr = 10

Ra	Kumar & Sood[16]			Kumar et al.[12]			Present study		
	C^*_{fX}	C^*_{fX}	Nu_x	C^*_{fX}	C^*_{fX}	Nu_x	C^*_{fX}	C^*_{fX}	Nu_x
0.8	0.72360	-0.71684	0.75538	0.74634	-0.76290	0.72319	0.74060	-0.76842	0.72038
1.5	0.76660	-0.74482	0.94473	0.783415	-0.79190	0.89982	0.783415	-0.77190	0.87982
2	0.84656	-0.94456	1.06360	0.80457	-0.80876	1.00945	0.88170	-0.74714	1.29496
3.5	0.84656	-0.79856	1.36360	0.85170	-0.84714	1.284 96	0.87180	-0.84914	1.31496

It is observed that ϕ drop in primary velocity and the corresponding boundary layer thickness as M, K, R, Ra, V_s and values rise in the FNF. While the opposite behavior is seen in Ra and values rise in NFNF. In this case, increasing the values of Ra and V_s causes the velocity magnitude to increase, enhancing the of the boundary layer and compressing the flow into a sheet, while increasing the values of M, K, R, and ϕ has the opposite effect on the velocity profiles. The magnetic field's Lorentz force causes a rise in viscous forces, which reduces the velocity of the nanofluid (U_1). The effects of M, K, R, Ra, and V_s on the secondary velocity profiles of Ag-water nanofluids and indicate an important change in the profiles with M, K, R, and ϕ in the FNF case, showing that the flow field may be changed by altering these parameters. The secondary velocity (V_1) profiles as well as the

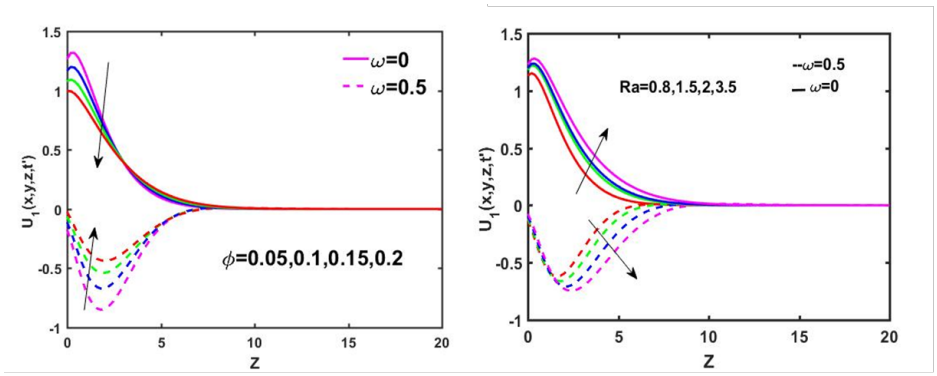

Figure 2(a) Figure 2(b)

Fig 2. Impact of distinct values of ϕ and *Ra* on Primary velocity profiles

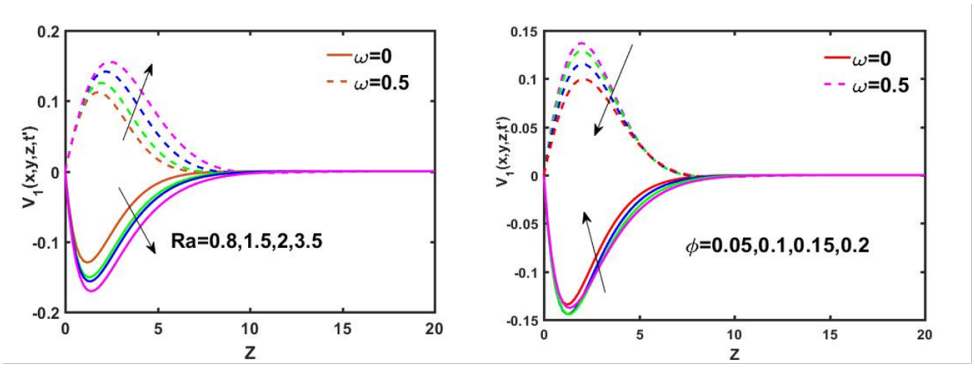

Figure 3(a) Figure 3(b)

Fig 3. Impact of distinct values of *Ra* and ϕ on Secondary velocity profiles

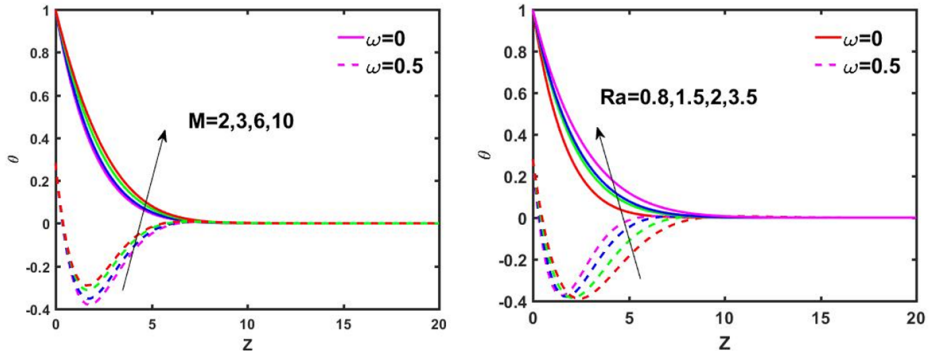

Figure 4(a) Figure 4(b)

Fig 4. Impact of distinct values of *M* and *Ra* on temperature profiles

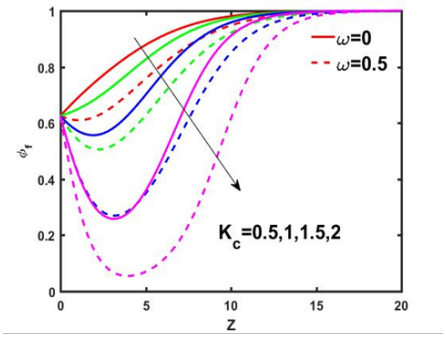

Figure 5(a)

Fig 5. Impacts of K_c and K_s on homogeneous species concentration (Φ_f)

thickness of the boundary layer are reduced in the case of FNF when the values of M, K, and ϕ are raised up, but they have been enhanced if the values of Ra, R, and V_s are pushed down.

Heat is transported by the emission of electromagnetic waves, which is known as thermal radiation. As shown in Figures 1, 2, 3, 4 and 5, greater values of the parameter of the radiation tend to slow down the heat transfer rate of fluid flow. Consequently, radiation efficiency controls thermal boundary layers since it has an advantage over conduction. The physical attraction point in this instance is the negative temperature profiles that developed in the FNF case as a result of the inverted Boltzmann distribution. Because energy states which are higher become more populated than the energy states which is lower when oscillation frequency has increased, this has a negative profile. The graphs for the NFNF scenario show that the dimensionless homogenous species concentration is a mono-tonically reducing function of M, K, R, and ϕ. Therefore, a rise in Ks will result in a decrease in the concentration of homogenous species. The concentration profiles of homogenous species in the FNF case are smaller than those in the NFNF case, as can be seen from all of these Figures. This may be caused by the vertical sheet's varying temperature, velocity, and rotations.

Table 2. Numerical outcomes for various values of significant parameters for skin friction coefficient (C^*_{fX}, C^*_{fy}) and Nusselt number Nu_x

Ra	V_s	Φ	Ec	FFNF Case (ω=0)			FNF Case (ω=0.5)		
				C^*_{fX}	C^*_{fy}	Nu_x	C^*_{fX}	C^*_{fy}	Nu_x
0.8	1	0.1	0.001	0.001985	-0.003299	1.484825	-0.062452	0.019067	2.591645
1.5				0.002293	-0.003455	1.666463	-0.060459	0.019246	2.914176
2				0.002473	-0.003516	1.785825	-0.059129	0.019267	3.691575
3.5				0.002882	-0.003705	2.106311	-0.055617	0.019062	3.691575
	0.01			0.004496	-0.003118	1.451680	-0.131197	0.011654	2.666473
	0.1			0.004033	-0.003151	1.457844	-0.119238	0.012941	2.660475
	0.5			0.002765	-0.003243	1.474595	-0.084665	0.016674	2.651141
	1.0			0.001985	-0.003299	1.484825	-0.061868	0.019141	2.650419
		0.05		0.002847	-0.002726,	1.507768	-0.062695	0.018058	2.652046
		0.1		0.001985	-0.003299	1.484825	-0.061868	0.019141	2.647419
		0.15		0.000951	-0.003749	1.466343	-0.062673	0.019221	2.634190
		0.2		-0.000305	-0.004095	1.452680	-0.064894	0.018551	2.630764
			0.001	0.009185	-0.003299	1.484825	-0.061868	0.019141	2.687419
			0.002	0.002021	-0.003313	1.464889	-0.061307	0.018886	2.671268
			0.004	0.002059	-0.003327	1.444630	-0.060760	0.018636	2.655545
			0.004	0.002097	-0.003342	1.424038	-0.060226	0.018391	2.640234

Table 3. Numerical outcomes for various values of significant parameters for Sherwood number ($Sh^*\Phi_f$, $Sh^*\Phi_s$)

Ra	V_s	K_c	K_s	FFNF Case ($\omega = 0$)		FNF Case ($\omega = 0.5$)	
				$Sh^*\Phi_f$	$Sh^*\Phi_s$	$Sh^*\Phi_f$	$Sh^*\Phi_s$
0.8	1	0.5	3.0	-0.064337	0.044054	0.023121	-0.022086
1.5				-0.067828	0.046837	0.025924	-0.024309
2				-0.069933	0.048524	0.027643	-0.025683
3.5				-0.074935	0.052554	0.038128	-0.029060
	0.01			-0.062503	0.042727	0.018488	-0.0181792
	0.1			-0.062843	0.042973	0.019447	-0.019486
	0.5			-0.063769	0.043643	0.022191	-0.021472
	1.0			-0.064337	0.044054	0.023977	-0.0018792
		0.5		-0.064337	0.067758	0.023977	-0.022763
		1.0		-0.057239	0.045289	0.029885	-0.028763
		1.5		-0.034337	-0.045169	0.123852	-0.110766
		2.0		-0.028537	-0.124054	0.228979	-0.122963
			0.5	-0.021157	0.015534	-0.002479	-0.001769
			1.0	-0.035714	0.025809	0.000257	-0.001953
			1.5	-0.046079	0.032797	0.005543	-0.005872
			2.0	-0.053738	0.037710	0.011791	-0.011610

4 Conclusion

This study made a comparison analysis of the two situations of NFNF and FNF in the Ag-water nanofluid 3-dimensional flow. Fluid temperature and homogeneous species concentration are severely hampered by oscillations in the velocity and temperature of the surface. Boosting *M, K,* ϕ and lowering *Ra* and V_s might delay boundary layer separations. As elevating *R, Ra,* ϕ*, M, K*, and *Ec*, temperature of the fluid is enhanced. In the FNF scenario, the flow field dissipates more heat than in the NFNF case. When comparing the FNF and NFNF scenarios, Φ_f is larger in the former. Temperature and surface velocity oscillations substantially reduce fluid temperature and concentration of homogenous species. Enhancing *M, K,* ϕ and decreasing *Ra* and V_s can delay boundary layer separations.

Though, the behavior is reversed for the Φ_f. In NFNF case, *M, K, R*, and ϕ have diminished effects, while V_s and *Ra* have increased effects on Φ_f. However, the effect has been reversed for the FNF case. If decreases in both cases with $K_c$and K_s *e*very trend is being reverse for Φ_s. In NFNF and FNF cases, magnified values of M result in a reduction in the magnitude of C^*_{fx}, C^*_{fy}, and Nu_x. In the NFNF case with K_c, $Sh^*\Phi_s$ is increased but $Sh^*\Phi_s$ is decreased. Boundary layers of homogeneous and heterogeneous are thicker in FNF case in comparison to NFNF case. In FNF case more heat is withdrawn from the flow field in comparison to NFNF case. Some practical implications of this work are the measurement of underground explosion intensity, processing of chemicals and materials, isotope separation, irrigation systems, rocket propulsion, filtering mechanisms, electronic device cooling, sweat cooling, heat exchangers.

References

1) Lund LA, Omar Z, Raza J, Khan I. Magnetohydrodynamic flow of Cu–Fe3O4/H2O hybrid nanofluid with effect of viscous dissipation: dual similarity solutions. *Journal of Thermal Analysis and Calorimetry*. 2021;143(2):915–927. Available from: https://doi.org/10.1007/s10973-020-09602-1.
2) Arulmozhi S, Sukkiramathi K, Santra SS, Edwan R, Fernandez-Gamiz U, Noeiaghdam S. Heat and mass transfer analysis of radiative and chemical reactive effects on MHD nanofluid over an infinite moving vertical plate. *Results in Engineering*. 2022;14:1–9. Available from: https://doi.org/10.1016/j.rineng.2022.100394.
3) Anuar NS, Bachok N, Arifin NM, Rosali H. Stagnation Point Flow and Heat Transfer over an Exponentially Stretching/Shrinking Sheet in CNT with Homogeneous–Heterogeneous Reaction: Stability Analysis. *Symmetry*. 2019;11(4):1–18. Available from: https://doi.org/10.3390/sym11040522.
4) Aslani KE, Mahabaleshwar US, Singh J, Sarris IE. Combined Effect of Radiation and Inclined MHD Flow of a Micropolar Fluid Over a Porous Stretching/Shrinking Sheet with Mass Transpiration. *International Journal of Applied and Computational Mathematics*. 2021;7(3):1–21. Available from: https://doi.org/10.1007/s40819-021-00987-7.
5) Jalili P, Azar AA, Jalili B, Ganji DD. Study of nonlinear radiative heat transfer with magnetic field for non-Newtonian Casson fluid flow in a porous medium. *Results in Physics*. 2023;48:1–27. Available from: https://doi.org/10.1016/j.rinp.2023.106371.
6) Hussain A, Alshbool MH, Abdussattar A, Rehman A, Ahmad H, Nofal TA, et al. A computational model for hybrid nanofluid flow on a rotating surface in the existence of convective condition. *Case Studies in Thermal Engineering*. 2021;26:1–12. Available from: https://doi.org/10.1016/j.csite.2021.101089.
7) Hussain A, Arshad M, Rehman A, Hassan A, Elagan SK, Ahmad H, et al. Three-Dimensional Water-Based Magneto-Hydrodynamic Rotating Nanofluid Flow over a Linear Extending Sheet and Heat Transport Analysis: A Numerical Approach. *Energies*. 2021;14(16):1–15. Available from: https://doi.org/10.3390/en14165133.
8) Nasirzadehroshenin F, Sadeghzadeh M, Khadang A, Maddah H, Ahmadi MH, Sakhaeinia H, et al. Modeling of heat transfer performance of carbon nanotube nanofluid in a tube with fixed wall temperature by using ANN–GA. *The European Physical Journal Plus*. 2020;135(2). Available from:

https://doi.org/10.1140/epjp/s13360-020-00208-y.
9) Shoaib M, Raja MAZ, Sabir MT, Islam S, Shah Z, Kumam P, et al. Numerical investigation for rotating flow of MHD hybrid nanofluid with thermal radiation over a stretching sheet. *Scientific Reports*. 2020;10(1):1–15. Available from: https://doi.org/10.1038/s41598-020-75254-8.
10) Farooq AA, Kahshan M, Saleem S, Rahimi-Gorji M, Al-Mubaddel FS. Entropy production rate in ciliary induced flows through cylindrical tubules under the consequences of Hall effect. *Journal of the Taiwan Institute of Chemical Engineers*. 2021;120:207–217. Available from: https://doi.org/10.1016/j.jtice.2021.03.024.
11) Khan SU, Shehzad SA. Electrical MHD Carreau nanofluid over porous oscillatory stretching surface with variable thermal conductivity: Applications of thermal extrusion system. *Physica A: Statistical Mechanics and its Applications*. 2020;550:124132. Available from: https://doi.org/10.1016/j.physa.2020.124132.
12) Kumar R, Kumar R, Koundal R, Shehzad SA, Sheikholeslami M. Cubic Auto-Catalysis Reactions in Three-Dimensional Nanofluid Flow Considering Viscous and Joule Dissipations Under Thermal Jump. *Communications in Theoretical Physics*. 2019;71(7). Available from: https://iopscience.iop.org/article/10.1088/0253-6102/71/7/779/meta.
13) Hussain M, Ashraf M, Nadeem S, Khan M. Radiation effects on the thermal boundary layer flow of a micropolar fluid towards a permeable stretching sheet. *Journal of the Franklin Institute*. 2013;350(1):194–210. Available from: https://doi.org/10.1016/j.jfranklin.2012.07.005.
14) Brinkman HC. The Viscosity of Concentrated Suspensions and Solutions. *The Journal of Chemical Physics*. 1952;20(4). Available from: https://doi.org/10.1063/1.1700493.
15) Khanafer K, Vafai K, Lightstone M. Buoyancy-driven heat transfer enhancement in a two-dimensional enclosure utilizing nanofluids. *International Journal of Heat and Mass Transfer*. 2003;46(19):3639–3653. Available from: https://doi.org/10.1016/S0017-9310(03)00156-X.
16) Kumar R, Sood S. Combined influence of fluctuations in the temperature and stretching velocity of the sheet on MHD flow of Cu-water nanofluid through rotating porous medium with cubic auto-catalysis chemical reaction. *Journal of Molecular Liquids*. 2017;237:347–360. Available from: https://doi.org/10.1016/j.molliq.2017.04.054.